Solar Energy 282 (2024) 112935

Contents lists available at ScienceDirect

Solar Energy

journal homepage: www.elsevier.com/locate/solener

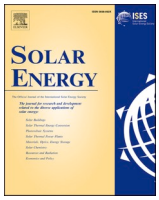

Efficiency improvement of ultrathin CIGS solar cells

Nour El I. Boukortt [a,b,*], Antonio Garcia Loureiro [a], Ahmad Abushattal [a]

[a] Centro Singular de Investigación en Tecnolooxías Intelixentes, University of Santiago de Compostela, Santiago de Compostela, Spain
[b] Department of Electronics and Information Systems, Ghent University, Technology Park 126, 9052 Zwijnaarde, Belgium

ARTICLE INFO

Keywords:
Ultrathin CIGS
TCAD
Rear-passivation
Fixed charge
Cell pitch

ABSTRACT

In this paper we present an optimization of rear-passivation parameters (cell pitch, opening width, and interface trap density) in u-CIGS solar cell using TCAD tools. The proposed investigation exhibits a significantly enhanced in understanding the beneficial effect of the rear passivation in ultrathin cell on conversion efficiency and reliability compared to existing solutions in the literature. Firstly, the device was calibrated according to the fabricated model taking in to account all material properties and defects at interfaces and within the bulk of the cells. Additional simulations demonstrate notable enhancements in cell performance due to changes in absorber thickness and doping concentration. However, traps were identified at rear u-CIGS/Al_2O_3 interface as a key factor degrading conversion efficiency by promoting carrier recombination. Mitigating this mechanism is essential for improving device performance. Incorporating a negative fixed charge density in the rear passivation layer offers a promising solution, providing effective field-effect passivation to minimize minority carrier recombination at the rear surface. The proposed u-CIGS solar cell device achieves an impressive efficiency of 15 % using a cell pitch of 1.5 μm and opening width of 300 nm with a fixed bandgap.

1. Introduction

Recent technological advancements, especially in photovoltaic materials and device configurations, have significantly accelerated the progress and implementation of renewable solar energy solutions. These advancements make sustainable energy more accessible and cost-effective [1–3], and are crucial for steering towards a sustainable future, mitigating the impending energy crisis, and curbing pollution, thereby contributing to global efforts for environmental preservation [1–3]. In addition, solar cell technology has been envisioned as a means of combating global warming and better greenhouse effects. Still, it largely awaits further improvement to be fully applied elsewhere. In the technology and development of solar cells, lightweight and ultrathin flexible solar cell devices such as thin-film Cu ($In_{1-x}Ga_x$) Se_2 solar cells are particularly attractive for their low manufacturing costs, minimal material requirements, flexibility of materials, and long-term stability [1–5]. CIGS solar cells have the importance of the absorber layer and the implication of the parameters by the thickness of the absorbing layer, doping concentration, and profile grading character of the Ga composition on the photovoltaic parameters [6]. CIGS has a tunable bandgap (E_g) in the range of 1.0–1.7 eV depending on the composition ratio x = Ga/(In + Ga). Therefore, thickness range of 2–3 μm is still being used with sufficient light absorption for CIGS absorber layer [3–5]. Thin-film CIGS solar cell technologies demonstrate high conversion efficiencies and have recently shown potential flexibility to be integrated as bottom cells in tandem configurations [6]. Different approaches have been focused on material properties, interfaces, and design configurations to enhance cell efficiency [5–12].

In 2024, Uppsala University reported a record conversion efficiency of 23.64 % for single thin-film Cu($In_{1-x}Ga_x$)Se_2 solar cells. This was achieved by implementing a 'hockey stick'-like GGI profile, maintaining a constant Ga content in the upper half of the absorber and a high concentration near the back contact, which effectively reduced V_{oc} losses [5]. The absorber was incorporated with a high silver amount. The reduction of CdS buffer layer thickness to 25 nm led to extensive light soaking in the absorber, enhancing the efficiency [5]. In 2019, Solar Frontier (SF) reached a record efficiency of 23.35 % [7,8], adding sulfur at the front surface of the CIGS which resulted in a gradual decrease in the valence band minimum and an increase in bandgap energy (E_g). This approach leads to reducing the hole concentration at the heterojunction and increases open circuit voltage [7,8,10].

In the last decade, many researchers have been investigating both experimentally and theoretically the case of CIGS thickness $d_{CIGS} \leq 500$ nm [1,13,14]. Reducing the absorber thickness below the standard

* Corresponding author at: Centro Singular de Investigación en Tecnoloxías Intelixentes, University of Santiago de Compostela, Santiago de Compostela, Spain.
E-mail address: nourelislam.boukortt@rai.usc.es (N.E.I. Boukortt).

https://doi.org/10.1016/j.solener.2024.112935
Received 22 July 2024; Accepted 11 September 2024
Available online 14 September 2024

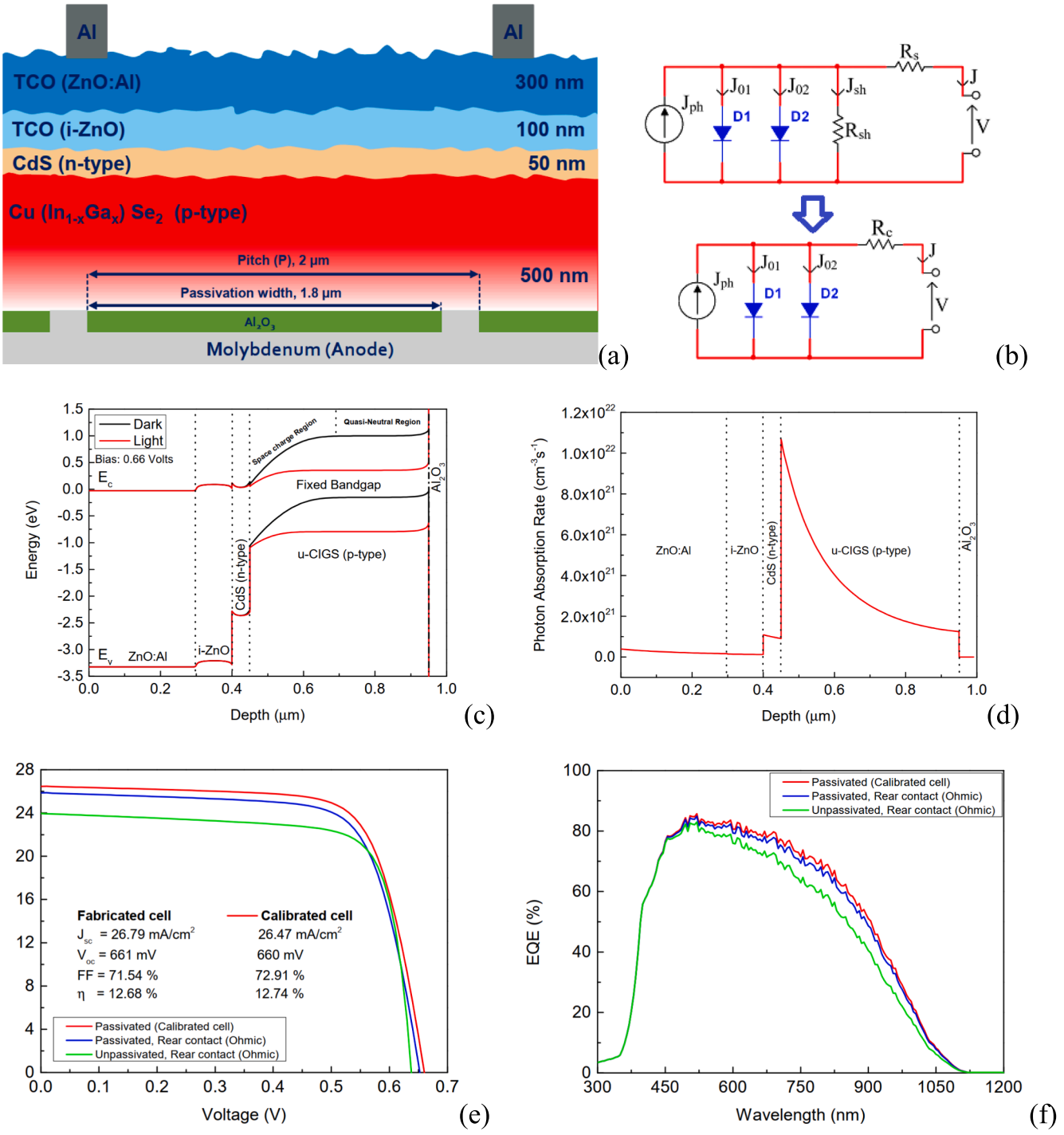

Fig. 1. (a) Cross-sectional of u-CIGS solar cell model. (b) Reduced equivalent electrical circuit for the two-diode PV model. (c) Corresponding energy band at V = 0.66 V. (d) Photo absorption rate across the cell. (e) J–V curves and corresponding characteristics of the calibrated solar cell. (f) EQE spectrum and integrated J of the optimized model.

micrometre scale (2–3 µm) has a benefit in reducing material costs and production time. Using thinner absorber layers in solar cells reduces light absorption and reveals degradation mechanisms that can negatively impact the cell's performance [15,16]. Therefore, ultrathin CIGS solar cells necessitate high-precision optimization strategies to improve photovoltaic performance. Many research approaches have been reported to improve the ultrathin CIGS solar cell performance [17–20].

This work presents numerical optimization of u-CIGS solar cells using TCAD tools. The main objective is to study the effect of rear passivation on device performance by improving light trapping and reducing transmission losses. Firstly, the u-CIGS device was calibrated according to the fabricated model taking in to account all material properties and defects at interfaces and within the bulk of the cells [1]. The impact of pitch cell, opening width, absorber thickness, doping concentration, negative fixed charge density ($-Q_f$) near the Al_2O_3/u-CIGS interface, and interface trap density (D_{it}) on cell performance has been studied. Studies have shown that D_{it} at the rear side (CIGS/Al_2O_3 interface) is critical for chemical passivation. D_{it} should be sufficiently low to reduce recombination losses in the CIGS device. The highest Q_f provides the best field effect passivation, thus improving cell efficiency.

The quality of the Al_2O_3 layer plays an important role, so it is necessary to take great care of this point. In this framework, there are various deposition techniques for Al_2O_3 thin films such as plasma-enhanced chemical vapor deposition (PECVD) [21], sputtering [22], atomic layer deposition (ALD) [23] and post-annealing [24] each of these techniques is characterized by positive and negative aspects that should be carefully evaluated when designing the cell growth process. Remarkably, efficiencies exceeding 15 % were achieved under precise simulation conditions for u-CIGS solar cells. Finally, the performance of these optimized solar cells was compared to recent studies, highlighting the key challenges faced by ultrathin devices in the photovoltaic field.

2. Electrical device modeling and simulation

Two-dimensional simulations were carried out using Silvaco ATLAS 2D, following the fabricated model reported by Jackson [1]. These simulations were carried out at room temperature, in darkness, and under illumination. The overall u-CIGS structure model is depicted in Fig. 1(a), comprises a configuration from top to bottom of ZnO/i-ZnO/CdS/CIGS/Al_2O_3/Molybdenum. In this model, a 500 nm p-type CIGS layer is the photo-absorbing layer, while the ZnO/i-ZnO (300/100 nm) and 50 nm n-type CdS layers act as window and buffer layers, respectively. Al-doped ZnO (AZO) layer used as transparent conducting oxide (TCO) due to its high transparency (>90 %) in the whole visible spectrum, low resistivity, low cost, non-toxicity, and good quality, even at room temperature deposition. The thin highly resistive intrinsic zinc oxide (i-ZnO) layer is required to protect the CdS/CIGS junction from damage during direct current (DC) sputtering of the highly conductive AZO film. The i-ZnO film plays an important role in improving the open-circuit voltage (V_{oc}) and fill factor (FF) by reducing the shunt paths due to its high resistivity. A 25 nm film of aluminum oxide (Al_2O_3) with contact openings has been introduced at the Mo/CIGS interface to serve as the rear surface passivation layer, containing $-Q_f$ to reduce rear surface recombination rates. The influence of this film on cell efficiency has been examined and clearly demonstrated in detail in our previous research work [25]. D_{it} is inserted into the model by donor-type Gaussian defect distribution at the CIGS/Al_2O_3 interface [1]. During deposition CIGS process on substrate, $MoSe_2$ layer is formed, the electrical properties are considered at Mo/CIGS interface. According to the literature, the front and back contact work functions were assumed 4.7 eV and 5.65 eV to approach real model as accurately as possible, respectively. A work function value used at Mo/CIGS interface forming an ohmic contact [1]. In addition, the electron/hole surface recombination velocity (SRV) at the electrodes were set to $S_n = S_p = 10^7$ cm/s. The contact resistance 0.181 Ω.cm^2 has been taken approximately by Jackson to imitate the series resistance (R_s) [1]. The total passivated model width (see Fig. 1) is 1 μm with the cell pitch (P) of 2 μm and initial contact hole of 200 nm (W, contact width). In ATLAS, alongside the electrical properties of each material, an AM 1.5 standard spectrum is utilized to illuminate the u-CIGS model. This takes into account both front and rear optical reflection to ensure an accurate determination of the model's realistic optical properties. The optical properties, such as the complex refractive indices (n, k), are sourced from the ATLAS library to faithfully represent light behaviour within the model. Key performance parameters include $-Q_f$ and D_{it}, which are instrumental in analyzing the influence of rear passivation on cell characteristics. The presence of a negative Q_f at the Al_2O_3/CIGS interface influences carrier densities (both electrons and holes) at the rear Mo/CIGS interface via internal electric field effects. D_{it} denotes the quantity of carrier traps formed at the Al_2O_3/CIGS interface, which can serve as recombination centers for electron-hole pairs. Fig. 1(c) shows the band diagram of the u-CIGS model in the dark and under illumination, with a fixed bias of 0.66 V. The conduction band bending, due to the presence of $-Q_f$ in the Al_2O_3 layer, is clearly observed highlighting that the rear passivation layer Al_2O_3 with $-Q_f$ can beneficially by the internal electric field (field-effect passivation) repel the minority carriers from rear recombination

Table 1
Comparison of simulation and experimental results for ultrathin CIGS solar cells [1].

PV characteristics	Measurement [1]	Simulation
J_0 (mA/cm^2)	–	5.29×10^{-7}
J_{sc} (mA/cm^2)	26.79	26.47
V_{oc} (mV)	661	660
P_{max} (W/m^2)	–	254.87
FF (%)	71.54	72.91
η (%)	12.68	12.74

[1]. The bending of energy in the valence band (E_v) arises from the accumulation of majority carriers (holes), namely holes. The extent of band bending is contingent upon the $-Q_f$ density present within the Al_2O_3 layer. This phenomenon leads to the formation of surface accumulation and/or inversion modes between CIGS and Al_2O_3 layers. The $-Q_f$ and D_{it} have previously been experimentally estimated to be in the range of -1×10^{12} cm^{-2} and 1×10^{11} cm^{-2}eV^{-1} at the CIGS/Al_2O_3 interface, respectively [1]. Fig. 1(d) presents photo absorption rate across the cell. The J–V curves and corresponding characteristics of the calibrated solar cell are presented in Fig. 1(e). The curve shows current density values corresponding to various voltage values, indicating favourable electrical behaviour at room temperature. A noticeable gain in the J_{sc} of 2.51 mA/cm^2 with passivated u-CIGS solar cell due to additional charge diffused from neutral-region through passivation layer was obtained. Fig. 1(f) illustrates the enhanced external quantum efficiency (EQE) of the u-CIGS model, attributed to enhanced rear photon scattering effects compared to the unpassivated model, specifically for 500 nm-thick CIGS absorber. Solar parameters are outlined in Table 1. In this model, the impact of D_{it} is incorporated using the surface recombination velocity (SRV) formula [1]:

$$SRV = \frac{U_s}{\Delta_n} \tag{1}$$

where,

$$U_s \cong \frac{(n_s p_s - n_i^2) \times q^{-1} v_{th} D_{it}}{\frac{n_s}{\sigma_p} + \frac{p_s}{\sigma_n}} \tag{2}$$

In this equation, U_S represents the recombination rate, while Δn denotes the excess carrier density. n_s/p_s and σ_n/σ_p represent the surface densities and cross-sections of electrons and holes, respectively. q represents the charge of the electron (1.6×10^{-19} C) and v_{th} represents thermal velocity. Due to the limitations of ATLAS, the model behaviour is simulated without considering the effects of shunt resistance (R_{sh}) and external series resistance (R_s). However, a contact resistance (R_c) in Ω·cm^2 has been incorporated at the Mo/CIGS interface, which directly emulates the series resistance of reference models. Dividing R_c by the contact area, it yields a full series resistance. This parameter calibration technique has achieved good results [1]. For the passivated solar cells, the contact interface exists only within the openings, covering a W/P ratio of the total cell area. R_s can be transformed into an equivalent R_c at the Mo/CIGS interface. This R_c accounts for the losses due to R_s, which depend on the size of the openings. The equivalent electrical circuit for the u-CIGS model is shown in Fig. 1(b). This approximation can be expressed by the following equation:

$$R_c = R_s \times \frac{W}{P} \tag{3}$$

Fig. 1(b) depicts a simplified model created in this investigation with ATLAS, which omits R_{sh} but incorporates R_c. Diode 1 and Diode 2 represent diffusion currents and generation/recombination (G/R) currents, respectively, and are defined by their current density J_0 and their nonideality factor n.

Applying Kirchhoff's Voltage Law (KVL) and Kirchhoff's Current Law (KCL) to the second equivalent circuit model under illumination (Fig. 1

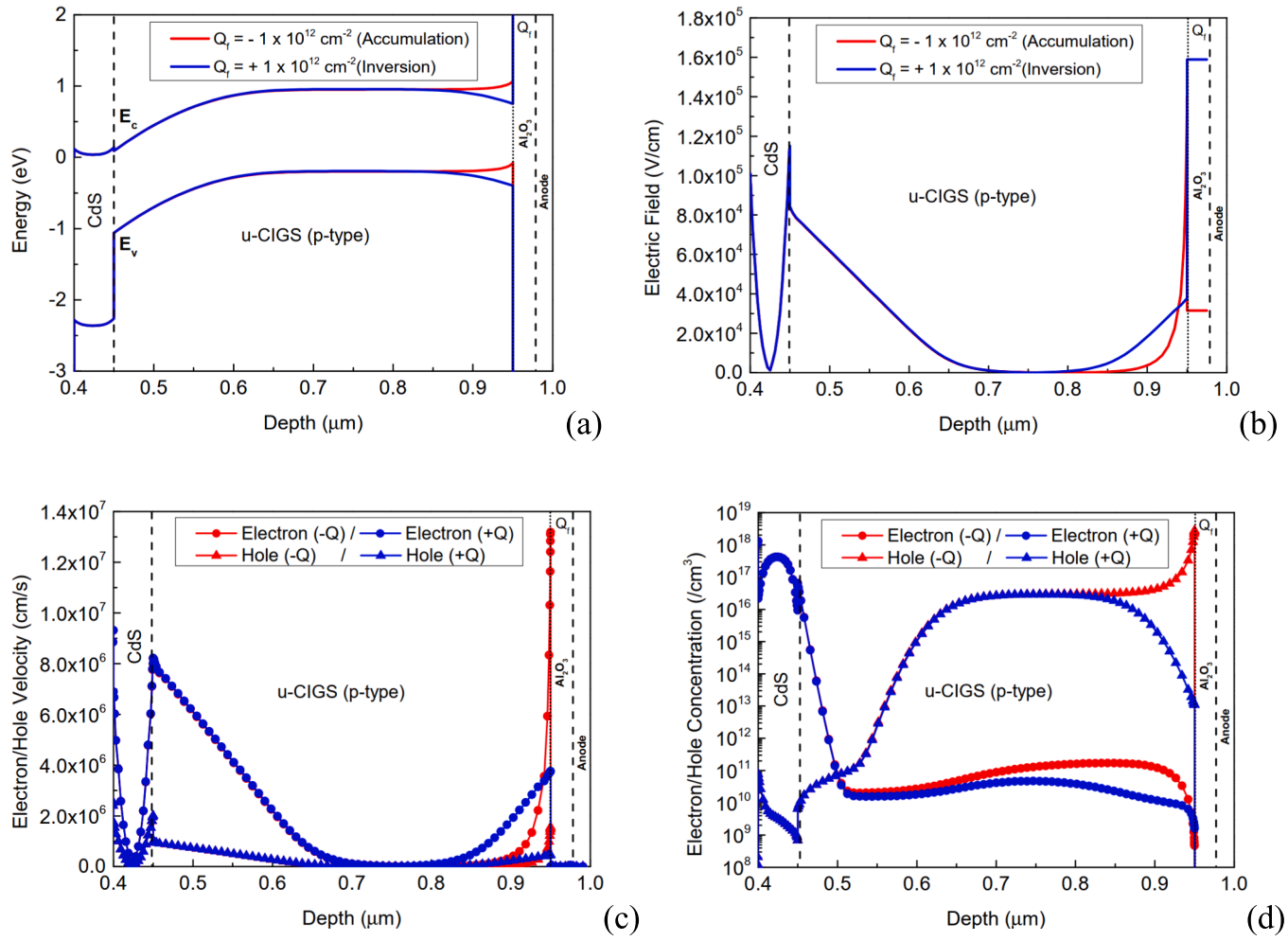

Fig. 2. (a) Bandgap diagram, (b) electric field, (c) electron/hole velocity, (d) electron/hole concentration in ultrathin CIGS model with rear-passivation.

(e2)), the resulting expression can be derived as follows:

$$J(V) = J_{PH} - J_{01}\left[e^{\left(\frac{q(V+R_cJ)}{n_1kT}\right)} - 1\right] - J_{02}\left[e^{\left(\frac{q(V+R_cJ)}{n_2kT}\right)} - 1\right] \quad (4)$$

Here, J represents the measured output current density, J_{PH} denotes the photocurrent density, V is the voltage, q is the electron charge, T stands for temperature, and k is the Boltzmann constant. Each diode in the model is assessed at suitable bias regions to differentiate the individual contributions to the total J. The simulation outcomes align well with the reference results [1].

3. Results and discussions

The primary aim of this research is to optimize the conversion efficiency of the ultrathin CIGS solar cell by investigating and understanding different approaches with regards to the fixed charge passivation, interface trap density, pitch cell, opening width, doping density and absorber thickness using TCAD tools. We have explored and underlying mechanisms associated with rear passivation in u-CIGS solar cells. Furthermore, this study provides useful predictions toward optimum design and accurate characterization for a complete solar cell structure model.

3.1. Rear passivation implementation with positive/negative fixed charge ($\pm Q_f$)

To fully exploit the advantage offered by the rear passivation, the cell model was initially calibrated based on a reference cell configuration. This reference cell comprised an Al_2O_3 layer of 25-nm-thick as the rear passivation, combined with a 500 nm thickness of CIGS (Absorber). In the fabrication process, a thin Al_2O_3 layer was deposited on top of Mo before the absorber deposition. In this framework, there are various deposition techniques for Al_2O_3 thin films such as plasma-enhanced chemical vapor deposition (PECVD) [21], sputtering [22], atomic layer deposition (ALD) [23] and post-annealing [24] each of these techniques are characterized by positive and negative aspects that should be carefully evaluated when designing the cell growth process. In the rear-passivation layer, there are rear contacts with opening diameters of 200 nm and placed at an equidistant pitch of 2 μm. Fig. 2 illustrates the effect of positive/negative fixed charge ($\pm Q_f$) on energy bandgap (a), electric field (b), and carrier's velocities (c) and concentration near CIGS/Al_2O_3 interface (d). Fig. 3 shows the effect of $\pm Q_f$ for different absorber thickness on cell performance. It's interesting to note the contrasting trends observed in the simulated cell parameters for positive and negative charges. At the interface, both chemical and field-effect passivation processes occur, impacting the behavior of charge carriers. Specifically, $-Q_f$ tends to induce accumulation of holes, while $+Q_f$ led to inversion of electrons. This effect of field passivation varies depending on the type of charge. High internal field effect passivation and minority carrier velocity are observed with $-Q_f$ which can prevent

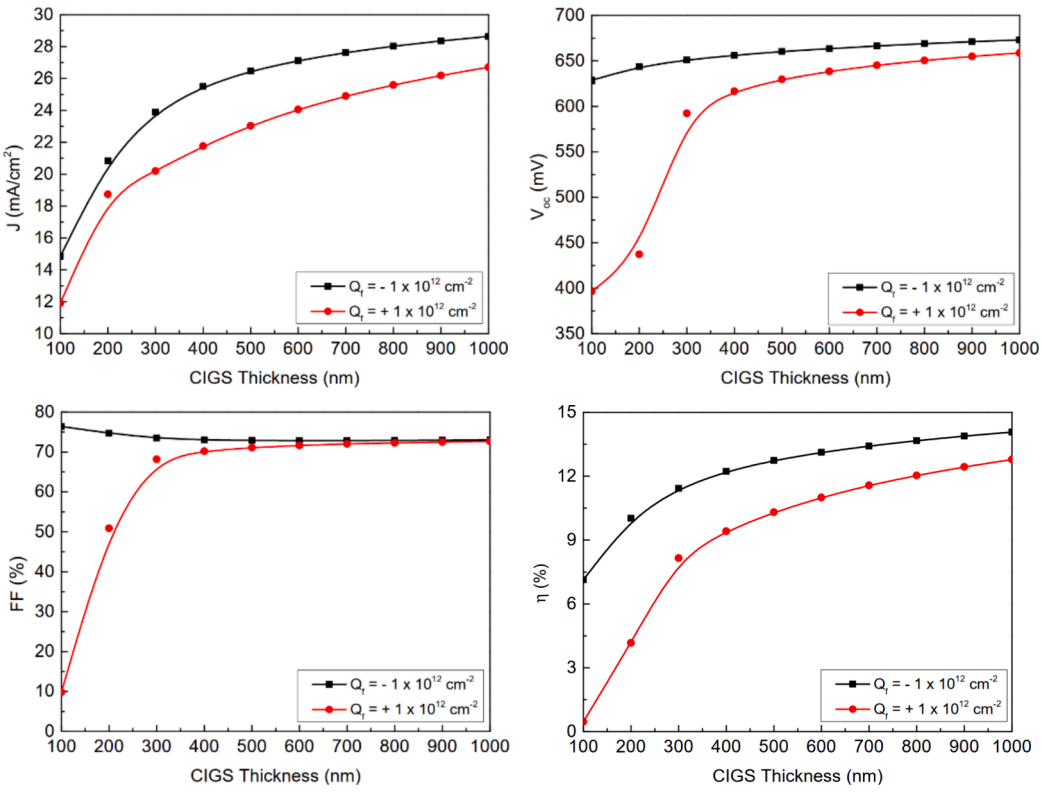

Fig. 3. Simulated parameters of u-CIGS solar cells, showing the variation in absorber thickness alongside $\pm Q_f$ densities, maintaining the D_{it} at 1×10^{11} $cm^{-2}eV^{-1}$ at CIGS/Al_2O_3 interface.

minority carriers (electron) to recombine near the surface. Repelled electrons can have a chance to be collected at front contact, thus enhancing J_{sc}. Passivation layer with positive fixed charge causes a decrease in minority carriers' velocity due to the high concentration giving a chance to be trapped or recombined near CIGS/Al_2O_3 interface (See Fig. 2(c and d)), thus degradation in cell performance. The SRV values of Mo/CIGS and CIGS/Al_2O_3 have been fixed at 10^7 $cm.s^{-1}$ to ensure electrical contact and 10^2 $cm.s^{-1}$, respectively. In Fig. 2(a), at CIGS/Al_2O_3 interface, the presence of band bending (depicted in blue) is notable. This bending occurs due to the attraction between $+Q_f$ and minority carriers (electrons), leading to the formation of an inversion layer (n-type) near the rear interface and depletion layer with p-type absorber. This mechanism facilitates the easy recombination of accumulated electrons at the rear contact openings, regardless of the absorber thickness. For higher intensities of positive fixed charges, where electrons accumulate at the rear absorber surface, a parasitic pseudo-PN-junction is formed with a built-in potential (V_{bi_rear}). This potential opposes the front CdS/CIGS junction (V_{bi_front}), resulting in an overall loss in the cell's $V_{oc} = (V_{bi\_front} – V_{bi\_rear})$, as depicted in Fig. 3(b). This figure shows higher losses in V_{oc} for lower absorber thicknesses compared to negative fixed charges. However, when the CIGS layer thickness is between 0.4 and 1 μm, the increase in efficiency as the absorber layer gets thicker is less pronounced, contributing to better cell efficiencies than those seen with layers thinner than 0.4 μm. Nonetheless, it should be acknowledged that the space charge region (SCR) of the front CdS/CIGS junction, which is approximately 200–300 nm, is situated nearer to the CIGS/Mo interface, where recombination is significant, leading to a discernible decrease in V_{oc} and overall cell efficiencies. The experiments involved varying the CIGS thickness from 0.1 μm to 1 μm while maintaining an interface trap density of 1×10^{11} $cm^{-2}eV^{-1}$ at the CIGS/Al_2O_3 interface. This series of experiments demonstrates the impact on passivated cells with $+Q_f$, particularly in thinner absorber thickness regimes (100–400 μm), compared to cells with $–Q_f$. This indicates the effective implementation of fixed charges in the Al_2O_3 layer, resulting in field-effect passivation. The presence of $+Q_f$ within the rear passivation layer can significantly impact device performance, particularly for u-CIGS layers. Conversely, cells with negative fixed charges exhibit higher performance. This is evident in the reduction of the rear surface SRVs from 1×10^7 cm/s to 1×10^2 cm/s. The decrease in the rear CIGS SRV was attributed to interface energy band bendings, as depicted in Fig. 2(a) [26–28].

3.2. Impact of -Q_f and absorber thickness/doping concentration on cell performance

The efficacy of cell performance can be significantly affected by rear passivation, exerting a profound influence on photogenerated charge carriers. In this scenario, $–Q_f$ is embedded within the bulk of the rear passivation layer for the calibrated u-CIGS model. Simulated device performances are evaluated for fixed cell pitch (2 μm), contact width (200 nm), and interface trap density (1×10^{11} cm^{-2} eV^{-1}) across varying CIGS absorber layer thicknesses and doping concentrations, considering different $–Q_f$ densities. The resulting plots for J_{sc}, V_{oc}, FF, and efficiency are illustrated in Figs. 4 and 5(a–d). These figures depict the substantial impact of $–Q_f$ on cell parameters amidst changes in absorber thickness and dopant concentration. Fig. 4(a) highlights notably low J_{sc} values for ungraded CIGS absorber thicknesses below 0.3 μm. Multiple factors are responsible for these phenomena, such as the inadequate absorption capability of the CIGS layer, the occurrence of recombination at the interface between the front CdS and CIGS layers, and recombination within the SCR. The SCR, specifically, is crucial for the collection of charge carriers, especially when the CIGS thickness is close to the width of the SCR. Typically, the electric field within the SCR facilitates the efficient collection of carriers generated by the light within the SCR, complemented by the diffusion of carriers from the neutral region of the CIGS, which lies outside the SCR [29]. An improvement in V_{oc}, J_{sc}, and η is observed specifically for thinner absorber layers (i.e. 0.1–0.6 μm). Increasing $–Q_f$ within the Al_2O_3 layer

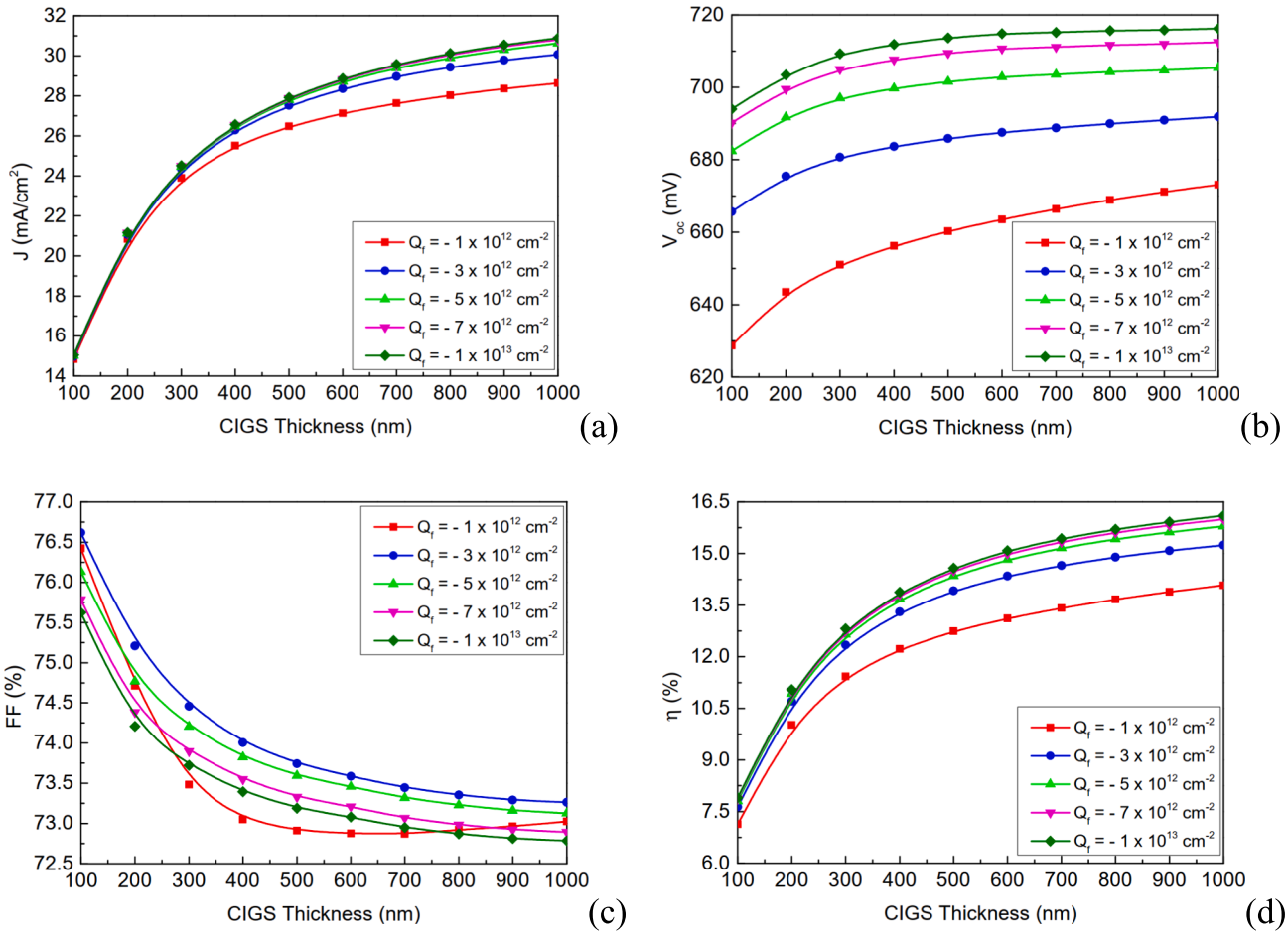

Fig. 4. Simulated parameters of u-CIGS solar cells, showing the variation in absorber thickness alongside $-Q_f$ densities, maintaining the D_{it} at 1×10^{11} $cm^{-2}eV^{-1}$ at CIGS/Al_2O_3 interface.

enhances the efficacy of shielding minority carriers, particularly electrons, from recombining with interface traps. The presence of $-Q_f$ establishes an internal electric field that deflects minority carriers away from the trap-laden CIGS/Mo interface, thereby bolstering cell efficiency. As the absorber thickness diminishes to below or near the bulk diffusion length ($L_d \approx 0.25$ μm, as commonly reported in literature) of minority carriers, particularly for thinner layers (<0.5 μm), there is a substantial increase in V_{oc} owing to a notable improvement in the effective diffusion length (resulting from an additional drift field) [30]. When the absorber layer's thickness is less than L_d, the J_{sc} decreases because the photocurrent diffusion component is effectively eliminated. This means the contribution to the photocurrent from regions beyond the SCR is lost. Consequently, device energy conversion efficiency improves due to the augmentation in J_{sc}. However, the enhancement in J_{sc} (Fig. 4(a)) and cell efficiencies (Fig. 4(d)) is anticipated to be more pronounced with slightly thicker absorbers (i.e., > L_d). In contrast, for thicker absorber layers than or equal to 1 μm, the impact of the additional drift field becomes less significant, thereby restricting gains in both J_{sc} (attributed to improve collection probability at the SCR) and V_{oc} (owing to reduced rear surface recombination at the rear contact). In addition, reducing the absorber thickness leads to reducing the bulk defect densities of absorber layer, and mitigating the impacts of non-radiative recombination, thereby improving overall recombination losses. The main parameters related to carrier recombination are V_{oc} and FF. Fig. 4 illustrates enhancements in J_{sc}, V_{oc}, and η across the applied thickness range, attributed to the presence of $-Q_f$ in the Al_2O_3 layer. Conversely, there is a negative impact on the FF due to an increase in series resistance throughout the device, highlighting an overall resistance issue. Notably, a significant increase in J_{sc} is evident for all models (varying Q_f) at lower thicknesses (~0.6 μm), where thick absorber films may lead to charge carriers recombining before reaching the electrodes, thereby reducing the collection probability at SCR. The impact of the rear passivation layer diminishes for thicker absorbers (beyond 0.8 μm), as most of the photons are absorbed by the absorber. However, in thinner absorbers, long wavelengths might not be adequately absorbed, yet minority carriers generated beyond the SCR are drifted towards the SCR due to the additional drift electric field (E_{drift}) induced by the high density of $-Q_f$ in the rear passivation. Conversely, a thicker absorber layer exacerbates optical losses, necessitating meticulous optimization of the u-CIGS layer in terms of thickness, doping concentration, defect density, and interface defect density. In ultrathin CIGS solar cells, recombination can occur in two distinct physical regions: the CIGS bulk and the rear passivation [31]. Here, the bulk doping density plays a crucial role in determining bulk resistivity (related to FF) and bulk lifetime (related to V_{oc}). Elevating the doping level in the absorber layer enhances cell performance by increasing the built-in electric field (V_{bi}) across the solar cell. Consequently, the doping level should be sufficiently high to facilitate the use of a very thin Al_2O_3 layer for effective passivation while minimizing optical losses. The photogenerated charge carriers' separation process can be improved by a strong V_{bi}, thus collection efficiency and fill factor. The impact of implementing high $-Q_f$ in the rear passivation layer on cell performance is observed clearly in Fig. 5. Note that J_{sc} is almost constant and independent of doping concentration for values less than 10^{16} cm^{-3}, as shown in Fig. 5a. At very high doping concentrations, the carrier density is increased, the effect Auger recombination becomes increasingly

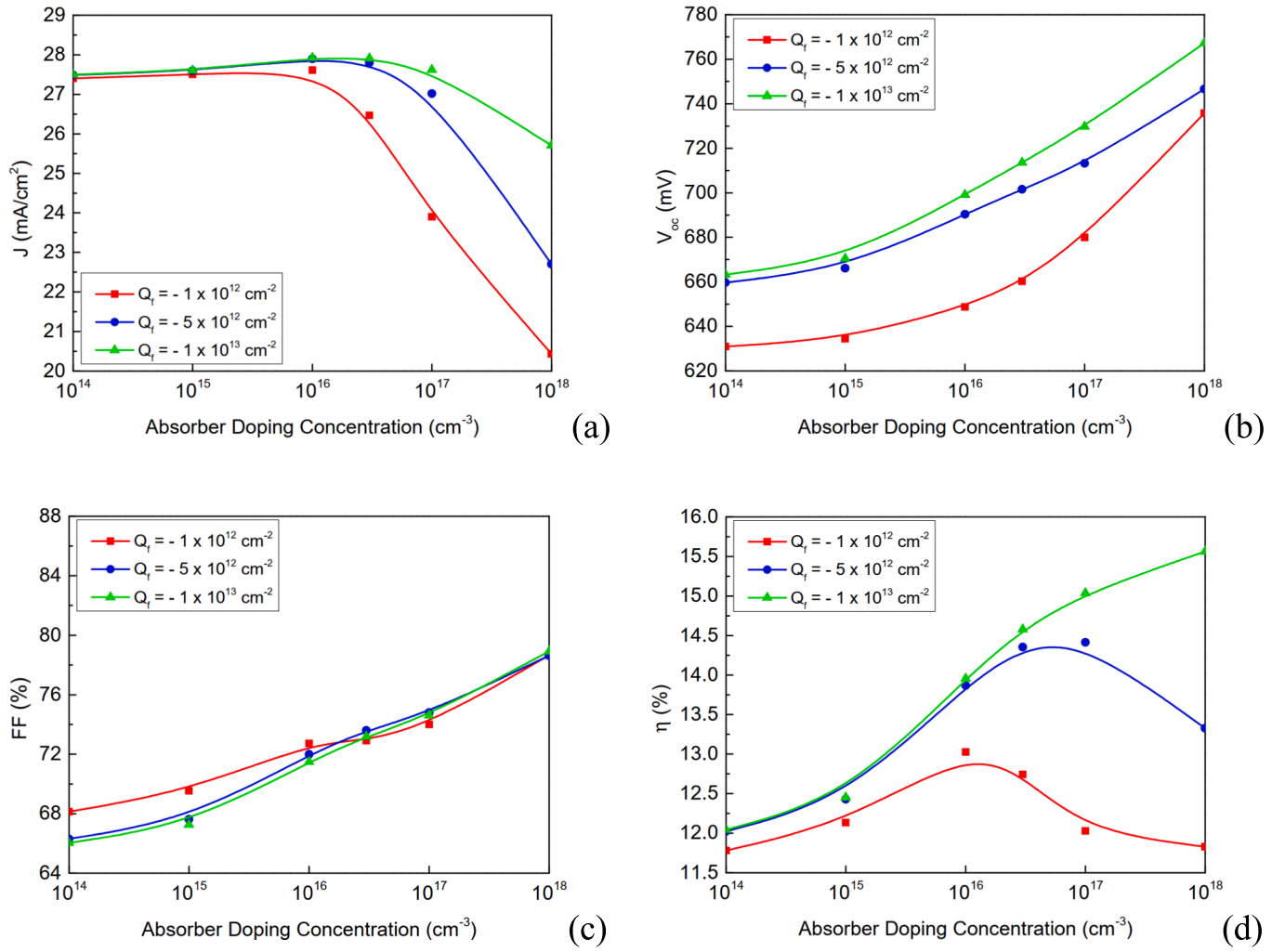

Fig. 5. Simulated parameters of u-CIGS solar cells, showing the variation in absorber doping concentration alongside different negative fixed charge densities, maintaining the D_{it} at 1×10^{11} $cm^{-2}eV^{-1}$ at CIGS/Al_2O_3 interface.

prominent, causing a decrease in cell performance. The recombination rate is contingent upon the concentration of minority carriers. A slight improvement in V_{oc} and FF with doping density can also be associated with a decrease in sheet resistance and an augmentation in the bulk lifetime of the absorber layer, respectively. This experiment demonstrates the beneficial impact of high $-Q_f$ for high doping density on cell performance. An implemented passivation layer with a high density of $-Q_f$ repels the minority carriers (electrons), thereby reducing surface recombination through the creation of an internal electric field. In addition to reducing the recombination rate, the dielectric layer also enhances reflection at the rear surface for certain thicknesses [31,32], thereby increasing the optical path as well. The SRV at the Al_2O_3/CIGS interface was fixed at 10^2 cm/s. The impact of implementing high $-Q_f$ in the rear passivation layer on cell performance is observed clearly from 10^{16} cm^{-3}. The efficiency results show an initial increase from low doping levels, where passivation has a significant effect on performance, particularly in V_{oc}. The improvement in performance continues until it reaches an optimal point, after which further increases in doping density result in a decline. This decline is attributed to the rise in bulk recombination within the absorber layer. For standalone devices, the optimum thickness and doping level for the CIGS absorber could be set between 400–700 nm and 10^{16}–10^{17} cm^{-3} for high efficiency, respectively. The results show maximum efficiency can be achieved >15 % for high density of $-Q_f$.

3.3. Opening width optimization for rear-passivated u-CIGS cells

In our previous study, we demonstrated the substantial effect of rear passivation with high negative charge density on cell performance. In passivated thin-film cells, the rear contact holes geometry size and distribution along the back side surface have been found important to investigate in order to achieve high cell efficiency. To achieve this, it's crucial to assess the influence of altering the opening width and negative charge density, both with rear contact resistance ($R_c = 0.1$ Ω·cm^2) and without ($R_c = 0$ Ω·cm^2), on the photovoltaic parameters. Same cell configuration was used in this section and has been simulated under AM1.5 illumination. The opening width was varied from 50–1000 nm at a fixed pitch size 2 μm and constant interface trap density 1×10^{11} $cm^{-2}eV^{-1}$. Moreover, two specific values of Q_f -1×10^{13} cm^{-2} and -1×10^{12} cm^{-2} have been considered at the CIGS/Al_2O_3 interface. As discussed earlier for passivated cells, current density can be improved when $-Q_f$ is high enough. However, when increasing the opening width, contact area of the passivated cells with high $-Q_f$, the current densities start decreasing due to effective recombination on the back surface at CIGS/ Mo interface. The trend in V_{oc} mirrors that of J_{sc}, with values surpassing those of the reference cell, particularly for narrower opening widths. When the rear contact area is smaller than the passivation area, the FF is degraded dramatically due to an increase of the series resistance across the cell and by the presence of the contact resistance as illustrated in Fig. 6(c) (red and blue curves). In this figure, when the rear

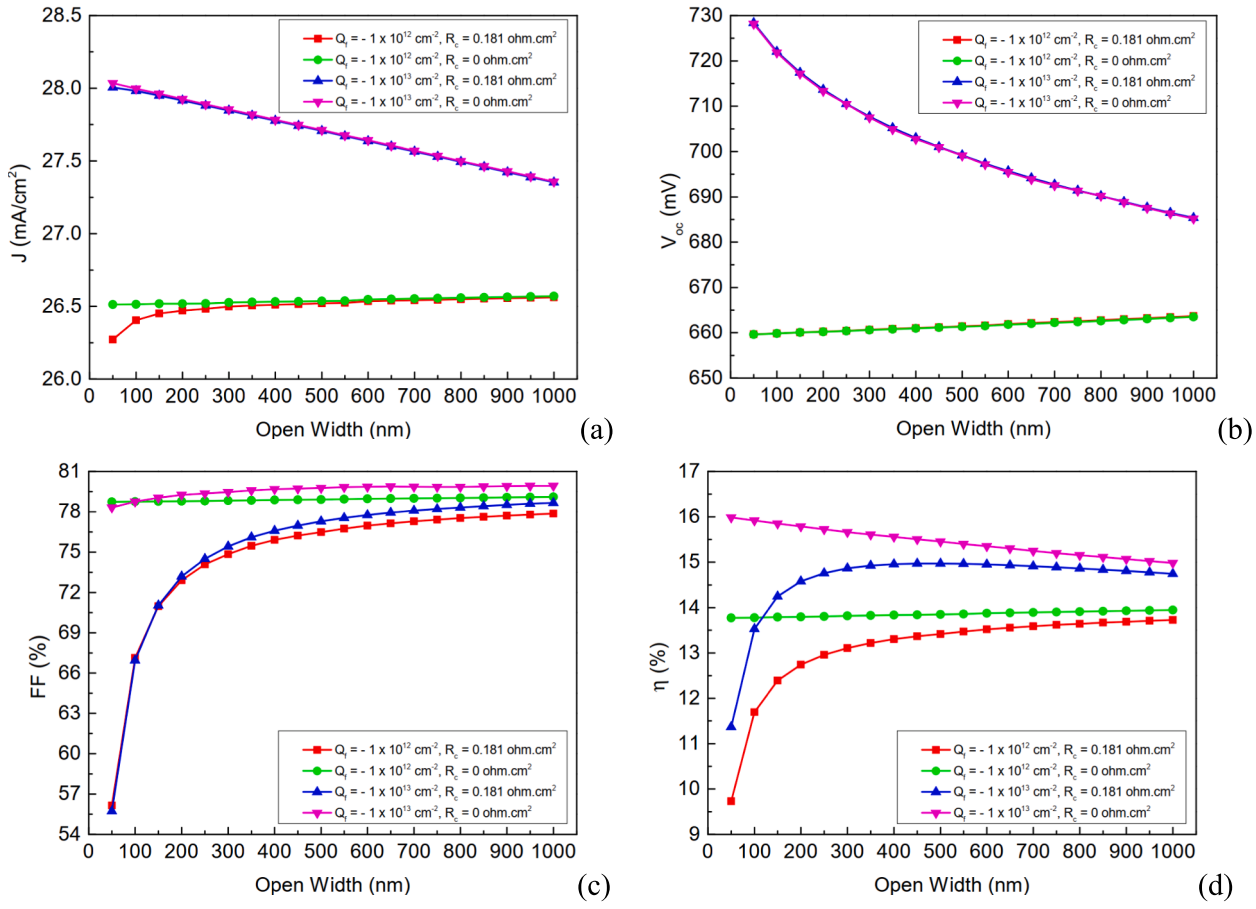

Fig. 6. Simulated parameters of u-CIGS solar cells, showing the variation in opening width alongside different negative fixed charge densities, maintaining the D_{it} at 1×10^{11} $cm^{-2}eV^{-1}$ at CIGS/Al_2O_3 interface.

contact area becomes larger, the FF is improved. The cell efficiency is influenced by all the mentioned PV parameters. With the presence of R_c and high $-Q_f$, the efficiency follows a similar trend as FF, which is considered a dominant factor for these specific cell models. Initially, the efficiency improves with smaller openings, where the effect of passivation significantly enhances cell performance, peaking at an optimal value of 14.97 % (as indicated by the blue curve). Beyond this point, further widening of the openings leads to a slight decrease in efficiency. The reduction in passivation area leads to increased recombination at the CIGS/Mo interface. The optimal efficiency is achieved within the range of 450 to 550 nm for a consistent hole pitch of 2 μm, which corresponds to an opening width-to-pitch ratio between 0.225 and 0.275. For lower Q_f (1×10^{12} cm^{-2}), all the positive impact of the passivation layer on cell performance that has been shown earlier are negated. In this case, as was earlier reported, with low fixed charge density, the cell can easily be degraded and reaching its limit due to not sufficient negative charge in the passivation layer. The sensitivity of cell performance to variations in opening width is clearly evident across different cell samples, considering the presence or absence of contact resistance and low or high $-Q_f$ density. This observation underscores the critical significance of high negative Q_f values, independent of other material and defect state variations. It highlights the importance of meticulously designing contact openings and minimizing contact resistance to achieve optimal performance in passivated cells.

3.4. Cell pitch sizes optimization for rear-passivated u-CIGS cells

In the preceding section, we have shown that the opening widths have a substantial influence on the cell's performance. This finding holds significant implications for cell design and offers valuable insights into the next steps in the fabrication process. Specifically, it suggests moving towards designs with larger opening grid sizes, which can reduce complexity and lower production costs while maintaining or even enhancing performance. However, various phenomena can occur during the fabrication processes, resulting variations in material properties and defects at interfaces or within the bulk of the cells. These various variations can either positively or negatively impact the cell performance. In passivated thin-film cells, the cell pitch size along the back side surface has been found important to optimize in order to make it less challenging during the fabrication process. For this purpose, it is important to quantify the impact of changing the cell pitch size and negative charge density with rear electrode as Schottky/Ohmic contact on PV parameters under AM1.5 illumination. The simulation results and their impact on photovoltaic (PV) performances are illustrated and summarized in Fig. 7. In this analysis, the cell pitch size was varied from 0.5–5 μm, maintaining a fixed opening width (W = 200 nm), and a constant interface trap density of 1×10^{11} $cm^{-2}eV^{-1}$ was applied. Additionally, two specific values of Q_f, -5×10^{12} cm^{-2} and -1×10^{12} cm^{-2}, were considered at the CIGS/Al_2O_3 interface. As discussed earlier for passivated cells, current density can be improved when $-Q_f$ is high enough. However, when increasing the cell pitch size, passivated area becomes larger than contact area, with high $-Q_f$ density, the current densities and open-circuit voltages start with a gradual increase due to internal electric field from passivation layer on the back surface at CIGS/Al_2O_3 interface, eventually reaching saturation as the cell pitch sizes become sufficiently high. In Fig. 7(b) (Red curve), a slight decrease in V_{oc} is noticeable, despite the passivation of the rear interface, while J_{sc} exhibits a slight increase for cell pitch sizes around 0.5–2 μm. On the

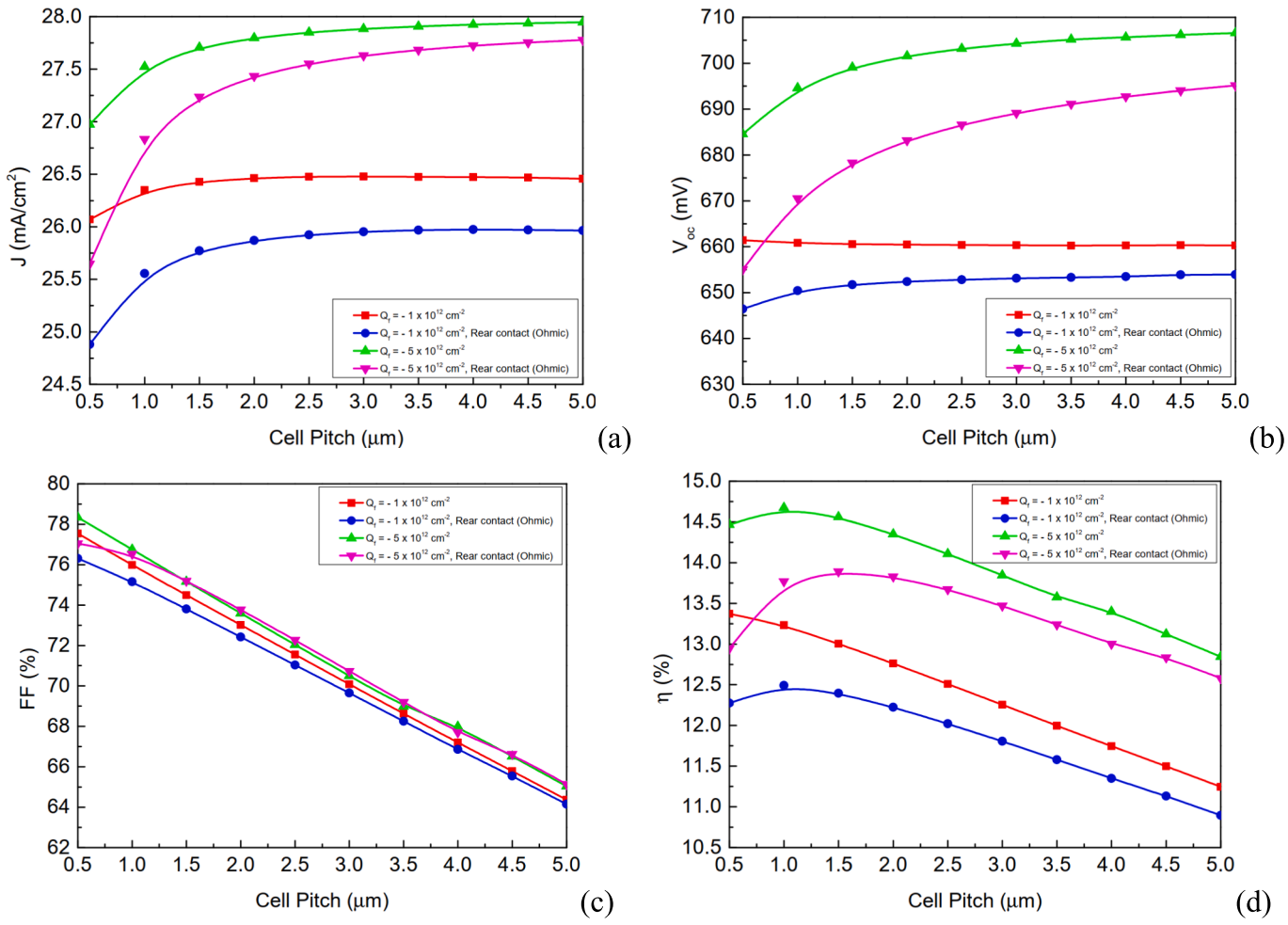

Fig. 7. Simulated parameters of u-CIGS solar cells, showing the variation in cell pitch size alongside different negative fixed charge densities and rear electrode as Schottky/Ohmic contact, maintaining the D_{it} at 1×10^{11} $cm^{-2}eV^{-1}$ at CIGS/Al_2O_3 interface.

other hand, at constant W, when the cell pitch size is larger than the contact area, the FF is degraded dramatically due to an increase of the series resistance across the cell as illustrated in Fig. 7(c). The cell efficiency is a combination of all mentioned PV parameters, with rear contact as Schottky/Ohmic contact and high $-Q_f$, the η increases from small pitch sizes, passes by an optimum value (14.67 % at 1 μm pitch, green curve) and then decreases slightly when the cell pitches are further increased. The significant enhancements observed in J_{sc} and V_{oc} are counteracted by substantial losses in FF due to high series resistance. An efficiency increases of approximately 1.3 %–1.4 % is achievable with an opening-to-pitch (W/P) ratio ranging from 0.13 to 0.4 for the studied cell configurations. These results underscore the necessity of having a negative Q_f exceeding 5×10^{12} cm^{-2} to attain reasonable cell efficiencies, particularly for ultra-thin CIGS absorbers with a thickness of 500 nm. Various outcomes may arise depending on the optimal value of the width-to-pitch ratio. For instance, Sozzi [33] conducted a simulation study where an optimal W/P ratio of 0.2 was identified, consistent with our findings. Jackson [1] also reported on both experimental and simulation studies, confirming an optimal W/P ratio of 0.2. This optimal discovery underscores the critical importance of controlling the design of the cell pitch and minimizing contact resistance for optimal performance.

3.5. Chemical passivation (D_{it}) analysis for rear-passivated u-CIGS cells

In the preceding sections, we explored how passivation parameters can influence cell performance, both positively and negatively. Additionally, another crucial parameter for evaluating the quality of the CIGS/Al_2O_3 interface is D_{it}. Therefore, it is essential to explore the influence of D_{it} on cell performance. In this analysis, typical values of $-Q_f$ within the rear passivation layer, such as 1×10^{13} cm^{-2}, 5×10^{12} cm^{-2}, and 1×10^{12} cm^{-2}, are considered, while D_{it} is varied from 1×10^{8} cm^{-2} eV^{-1} to 3×10^{12} cm^{-2} eV^{-1}. Initially, interface defects are linked to imperfect passivation, emphasizing the need for an appropriate growth process to keep the interface defect density below 10^{11} cm^{-2} for high performance. As previously discussed, in the case of passivated cells, an increase in cell performance can be achieved when the negative charge ($-Q_f$) is sufficiently high. The influence of D_{it} on PV performance has been simulated and summarized in Fig. 8. The cell pitch size and opening width remain fixed at 2 μm and 200 nm, respectively. From the results, it's evident that the influence of D_{it} depends on the negative fixed charge for D_{it} densities exceeding 1×10^{11} cm^{-2} eV^{-1}. There's a noticeable impact on cell performance for $Q_f = -1 \times 10^{11}$ cm^{-2}, particularly pronounced if the absorber thickness is thinner or closer to the SCR width (of the top junction), which would be influenced by the proximity to a highly recombinative rear trap-rich interface [34]. This high recombination is caused eventually by less impact of the field-effect passivation on minority carriers with larger D_{it}. To address these issues, having high $-Q_f$ within Al_2O_3 may help compensate for the recombination process induced by field passivation. Nevertheless, for larger $D_{it} > 1 \times 10^{12}$ eV^{-1} cm^{-2}, minimal impact on device performance losses can be observed for high $-Q_f$ densities. Achieving high performance requires $-Q_f$ to be sufficiently high to facilitate strong field-induced passivation and maintain low D_{it} for effective chemical passivation at

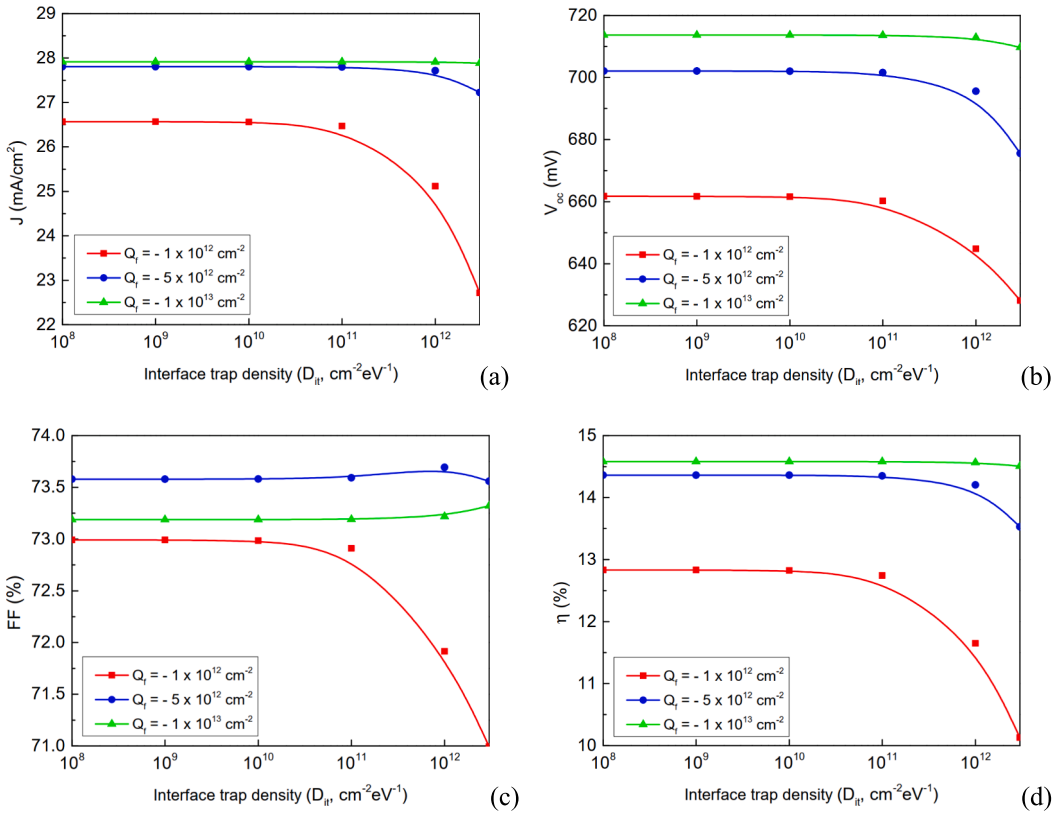

Fig. 8. Simulated parameters of u-CIGS solar cells, showing the variation in interface trap density alongside different negative fixed charge densities, maintaining the cell pitch size and opening width at 2 μm and 200 nm, respectively.

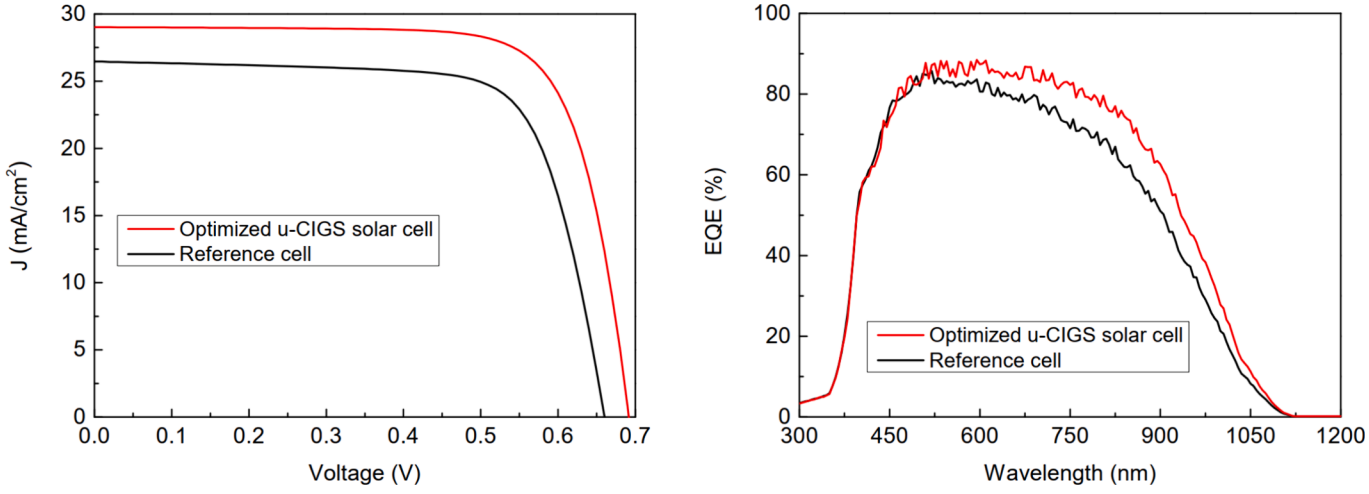

Fig. 9. J–V curves and EQEs of optimized u-CIGS models compared to reference model.

rear side. This investigation explored the impact of rear passivation properties on various photovoltaic (PV) parameters using TCAD tools.

3.6. Optimization of thin-film solar cell

With the aim of accelerating the achievement of high device efficiency within a short timeframe, recent significant research findings are integrated in this study. Utilizing numerical modeling to refine the ultrathin CIGS structure not only boosts device efficiency but also enhances its stability. This study highlights a strong correlation between simulation outcomes and experimental data for standalone solar cells [1,25]. For high cell efficiency, MgF_2 is used as an antireflection coating (ARC) layer to enhance photon absorption. Recently, many researchers are suggesting relocating MgF_2 ARC from its current position to the outer surface on the top of the glass to boost photons absorption [35]. The best efficiency obtained with the standalone u-CIGS solar cells was 15 %, achieved by optimizing the parameters, including the cell pitch size, opening width, negative fixed charge, and minimizing the rear passivation layer's interface trap density. In addition, we have used 1.5 μm cell pitch, 300 nm opening width, 1×10^{16} cm^{-3} acceptor doping density, 1×10^{10} cm^{-2} eV^{-1} interface trap density CIGS/ Al_2O_3 interface, and Molybdenum as the back contact to control the incoming light at the rear surface under the passivation layer with high negative fixed charge with within the passivation layer (Al_2O_3), about -1×10^{13} cm^{-2}; This

Table 2
Characteristics for the investigated u-CIGS models.

u-CIGS Models	J_{sc} (mA/cm^2)	V_{oc} (mV)	FF (%)	η (%)
Optimized cell (ARC MgF_2/Glass)	29.01	691.48	75.00	**15.05**
Optimized cell (ARC Glass)	28.80	691.23	75.01	14.93
Optimized cell (ARC MgF_2)	28.31	690.65	75.03	14.67
Reference cell (Calibrated)	26.47	660	72.90	12.74
Our previous work [31]	28.56	625.5	74.85	13.37
Experiment/Simulation [1]	26.79	661.6	71.54	12.68
Experiment/Simulation [36]	21 ± 0.1	592 ± 3	68 ± 3	8.1 ± 0.1

strategy allows us to get a significant enhancement in J_{sc} and V_{oc}. Fig. 9 illustrates J–V curves and EQEs of the optimized ultrathin-film CIGS structure compared to the reference cell (Calibrated model). The high efficiency was enabled by a high short-circuit current density of 29 mA/cm^{-2} and excellent FF, exceeding 75 %. The open-circuit voltage at 691.48 V. Table 2 summarizes the PV cell performance of the investigated models in comparison to recently published work [1,31].

4. Conclusion

This paper conducted numerical simulations of ultrathin-film CIGS solar cells using a TCAD simulator. To ensure high reliability conditions, standalone u-CIGS solar cell models have been calibrated according to the fabricated device leading to high accuracy of the simulation results. After device validation, the only way to enhance the efficiency is by improving the J_{sc} and V_{oc} which are limited by recombination mechanisms in the front/back absorber surface. We focused on understanding how the rear surface passivation in CIGS solar cell strong impact has on cell performance as a function of cell pitch, opening width, absorber thickness, doping concentration, negative fixed charge density, and interface trap density. The results of this study significantly enhance the understanding of the role of the investigated parameters in enhancing the cell performance. Nevertheless, excessive absorber thickness, doping concentration, and interface trap density are found to correlate with higher device resistivity, increased bulk carrier recombination rates, and elevated recombination losses at the rear metal contact. Overall, this study offers guidelines for achieving cell efficiencies exceeding 15 % for ultrathin CIGS solar cells by considering various recombination mechanisms and passivation properties.

CRediT authorship contribution statement

Nour El I. Boukortt: Conceptualization, Investigation, Methodology, Resources, Software, Writing – original draft, Writing – review & editing. **Antonio Garcia Loureiro:** Resources, Software, Supervision, Writing – review & editing. **Ahmad Abushattal:** Resources, Visualization, Writing – review & editing.

Declaration of Competing Interest

The authors declare that they have no known competing financial interests or personal relationships that could have appeared to influence the work reported in this paper.

Acknowledgement

The authors declare no competing financial interests.

References

[1] J. Lontchi, M. Zhukova, M. Kovacic, et al., Optimization of back contact grid size in Al2O3-rear-passivated ultrathin CIGS PV cells by 2-D simulations, IEEE J. Photovoltaics 10 (6) (2020) 1908–1917.
[2] M.A. Green, D.E. Dunlop, J. Hohl-Ebinger, M. Yoshita, N. Kopidakis, A.W.Y. Ho-Baillie, Solar cell efficiency tables (Version 55), Prog. Photovolt. Res. Appl. 28 (1) (2020) 3–15.
[3] N. Boukortt, S. Patanè, Single junction-based thin-film CIGS solar cells optimization with efficiencies approaching 24.5%, Optik 218 (2020) 165240.
[4] B. Vermang, J.T. Wätjen, C. Frisk, V. Fjällström, F. Rostvall, M. Edoff, P. Salomé, J. Borme, N. Nicoara, S. Sadewasser, Introduction of Si PERC rear contacting design to boost efficiency of Cu (In, Ga) Se_2 solar cells, IEEE J. Photovoltaics 4 (6) (2014) 1644–1649.
[5] J. Keller, K. Kiselman, N.M. Olivier Donzel-Gargand, M.B. Martin, O. Lundberg, E. Wallin, L. Stolt, M. Edoff, High-concentration silver alloying and steep back-contact gallium grading enabling copper indium gallium selenide solar cell with 23.6% efficiency, Nat. Energy (2024), https://doi.org/10.1038/s41560-024-01472-3.
[6] J. Zheng, C. Xue, G. Wang, et al., Efficient flexible monolithic perovskite–CIGS tandem solar cell on conductive steel substrate, ACS Energy Lett. 9 (4) (2024) 1545–1547.
[7] M. Nakamura, et al., Cd-free Cu(In,Ga)(Se,S)$_2$ thin-film solar cell with record efficiency of 23.35%, IEEE J. Photovolt. 9 (2019) 1863–1867.
[8] H. Sugimoto, H. Tomita, K. Yamaguchi, Y. Hirai, T. Kato, High-performance near-stoichiometric Cu(In,Ga)Se_2 solar cells by sub-percent Ag-doping, in: 29th PVSEC Conference, pp. 723–726 (PVSEC, 2019).
[9] M.A. Green, Do built-in fields improve solar cell performance? Prog. Photovolt. Res. Appl. 17 (2009) 57–66.
[10] T. Kobayashi, et al., Impacts of surface sulfurization on Cu(In_{1-x}, G_ax)S_e2 thin-film solar cells, Prog. Photovolt. Res. Appl. 23 (2015) 1367–1374.
[11] E. Avancini, et al., Impact of compositional grading and overall Cu deficiency on the near-infrared response in Cu(In, Ga)S_e2 solar cells, Prog. Photovolt. Res. Appl. 25 (2017) 233–241.
[12] T.M. Friedlmeier, et al., Improved photocurrent in Cu(In,Ga)Se_2 solar cells: from 20.8% to 21.7% efficiency with CdS buffer and 21.0% Cd-free, IEEE J. Photovolt. 5 (2015) 1487–1491.
[13] R. Kotipalli, et al., Influence of Ga/(Ga + In) grading on deep-defect states of Cu (In, Ga)S_e2 solar cells, Phys. Status Solidi RRL 9 (2015) 157–160.
[14] J. Krc, M. Sever, A. Campa, Z. Lokar, B. Lipovsek, M. Topic, Optical confinement in chalcopyrite based solar cells, Thin Solid Films 633 (2017) 193–201, https://doi.org/10.1016/j.tsf.2016.08.056.
[15] J. Goffard et al., Nanostructured back mirror for ultra-thin CIGS solar cells, in: Proc. 31th Eur. Photovolt. Sol. Energy Conf., pp. 1050–1052, 2015.
[16] N. Naghavi, et al., Ultrathin Cu(In, Ga)Se_2 based solar cells, Thin Solid Films 633 (2017) 55–60.
[17] O. Lundberg, M. Edoff, L. Stolt, The effect of Ga-grading in CIGS thin film solar cells, Thin Solid Films 480–481 (2005) 520–525.
[18] S. Schleussner, U. Zimmermann, T. Wätjen, K. Leifer, M. Edoff, Effect of gallium grading in Cu(In, Ga)Se2 solar-cell absorbers produced by multi-stage co-evaporation, Sol. Energy Mater. Sol. Cells 95 (2011) 721–726.
[19] M. Edoff, S. Schleussner, E. Wallin, O. Lundberg, Technological and economical aspects on the influence of reduced Cu(In, Ga)Se2 thickness and Ga grading for co-evaporated Cu(In, Ga)Se2 modules, Thin Solid Films 519 (2011) 7530–7533.
[20] W.-C. Chen, L. Stolt, M. Edoff, Ga/(Ga + In) grading effects on ultra-thin (UT) CIGS solar cell, in: Proc. IEEE Photovolt. Spec. Conf., Jun. 2019.
[21] D. Ledinek, P.M.P. Salomé, C. Hägglund, U. Zimmermann, M. Edoff, Rear contact passivation for high bandgap Cu(In Ga)Se 2 solar cells with a flat Ga profile, IEEE J. Photovolt. 8 (3) (2018) 864–870.
[22] P.M.P. Salomé, et al., Passivation of interfaces in thin film solar cells: understanding the effects of a nanostructured rear point contact layer, Adv. Mater. Interfaces 5 (2) (2018) 1701101.
[23] J. Goffard, et al., Light trapping in ultrathin CIGS solar cells with nanostructured back mirrors, IEEE J. Photovolt. 7 (5) (2017) 1433–1441.
[24] S. Yun, Y. Qin, A.R. Uhl, N. Vlachopoulos, M. Yin, D. Li, X. Han, A. Hagfeldt, New-generation integrated devices based on dye-sensitized and perovskite solar cells, Energ. Environ. Sci. 11 (2018) 476–526.
[25] N.E.I. Boukortt, S. Patanè, Y.M. et Abdulraheem, Numerical investigation of CIGS thin-film solar cells, Sol. Energy 204 (2020) 440–447.
[26] W. Shockley, W.T. Read, Statistics of the recombinations of holes and electrons, Phys. Rev. 87 (1952) 835, https://doi.org/10.1103/PhysRev. 87.835.
[27] A.G. Aberle, S. Glunz, W. Warta, Impact of illumination level and oxide parameters on Shockley–Read–Hall recombination at the Si-SiO2 interface, J. Appl. Phys. 71 (1992) 4422, https://doi.org/10.1063/1.350782.
[28] G. Dingemans, W.M.M. Kessels, Status and prospects of Al2O3-based surface passivation schemes for silicon solar cells, J. Vac. Sci. Technol. A 30 (2012) 040802, https://doi.org/10.1116/1.4728205.
[29] L.A. Kosyachenko, Possibilities to decrease the absorber thickness reducing optical and recombination losses in CdS/CdTe solar cells, Mater. Renewable Sustainable Energy 2 (2013) 1–20.
[30] O. Lundberg, M. Bodegard, J. Malmstrom, M. Stolt, Influence of the Cu(In, Ga) Se2 thickness and Ga grading on solar cell performance, Prog. Photovolt. Res. Appl. 11 (2003) 77–88.
[31] N.E.I. Boukortt, S. Patanè, M. Adouane, R. AlHammadi, Numerical optimization of ultrathin CIGS solar cells with rear surface passivation, Sol. Energy 220 (2021) 590–597, https://doi.org/10.1016/j.solener.2021.03.078.
[32] R. Kotipalli, et al., Addressing the impact of rear surface passivation mechanisms on ultra-thin Cu(In, Ga)Se2 solar cell performances using SCAPS 1-D model, Sol. Energy 157 (2017) 603–613, https://doi.org/10.1016/j.solener.2017.08.055.

[33] G. Sozzi, S.D. Napoli, M. Carrisi, R. Menozzi, Assessing the impact of rear point-contact/passivation on CIGS cells with different absorber thickness and grading, in: Proc. IEEE 7th World Conf. Photovolt. Energy Convers., 2018, pp. 3044–3047.
[34] O. Poncelet, R. Kotipalli, B. Vermang, A. Macleod, L.A. Francis, D. Flandre, Optimization of rear reflectance in ultra-thin CIGS solar cells towards > 20% efficiency, Sol. Energy 146 (2017) 443–452, https://doi.org/10.1016/j.solener.2017.03.001.
[35] L. Xu, J. Liu, F. Toniolo, M. De Bastiani, M. Babics, W. Yan, F. Xu, J. Kang, T. Allen, A. Razzaq, E. Aydin, Monolithic perovskite/silicon tandem photovoltaics with minimized cell-to-module losses by refractive-index engineering, ACS Energy Lett. 7 (7) (2022) 2370–2372.
[36] J. Krc, G. Cernivec, A. Campa, et al., Optical and electrical modeling of Cu(In, Ga) S_e2 solar cells, Opt. Quant. Electron. 38 (2006) 1115–1123, https://doi.org/10.1007/s11082-006-9049-1.